2018 European Control Conference (ECC)
June 12-15, 2018. Limassol, Cyprus

Global Observability Analysis of Aided-INS for UAVs Equipped with Visual Odometry Systems

Alessandro Bosso, Nicola Mimmo, Christian Conficoni, Andrea Tilli

Abstract— **In this work, observability properties of Inertial Navigation Systems aided with Global Navigation Satellite Systems and Visual Odometry are investigated and applied to the case of UAVs. A global analysis is carried out exploiting the concept of indistinguishable trajectories, that are characterized by solutions of Differential Algebraic Equations. A hybrid formulation is presented to combine two different indistinguishable dynamics, which arise depending on vehicle speed. For particular scenarios commonly encountered in practice, explicit conditions on the system inputs are obtained and appropriately cast as persistency of excitation requirements. With the presented tools, the benefits from Visual Odometry in enhancing observability can be appreciated, in particular w.r.t. attitude and bias estimation, and useful practical indication on the kind of maneuvers making the system observable can be drawn. Assessment of the theoretical results is provided by means of realistic numerical simulations, tailored to the considered UAV application.**

I. Introduction

Inertial Navigation Systems (INS) have been a core element for several military and civilian applications for long time. Nowadays, the most popular architecture is based on Inertial Measurement Units (IMUs), mounted rigidly on the vehicle in a so-called strap-down configuration [1]. Typically, the low-cost inertial sensors (e.g. accelerometers, gyroscopes) IMUs are equipped with suffer from noise and biases, affecting long term accuracy. For this reason, navigation is commonly aided by means of external instrumentation such as Global Navigation Satellite Systems (GNSS) and/or vision devices. Given the large number of autonomous vehicles expected in the near future, the quest for reliable navigation algorithms, exploiting the aforementioned sensor technologies to reconstruct the moving object state, is growing.

In this respect, regardless of the estimation method, a crucial aspect concerns observability analysis, as it provides rigorous results of what kinematic states can be reconstructed, despite measurement non-idealities. However, such study comes with some challenges, given by the non-linear time-varying nature of system mechanization dynamics. Several approaches have been proposed in the literature. In [2], [3] system linearization and particular conditions making it time invariant are considered for flying and land vehicle applications, respectively, and the standard observability matrix rank test is applied. In [4] linear time-varying dynamics, obtained neglecting position error, are handled with a Lyapunov transformation and the study of an equivalent system. In [5], instantaneous observability of the time-varying dynamics of INS aided with multiple antenna GPS is investigated, while [6] studies the GPS-aided INS observability Gramian properties under specific working conditions.

A popular method to perform state reconstruction, based on the seminal work [7], exploits the computation of Lie derivatives of the output functions to apply a rank test to the observability matrix, obtained by differentiating such derivatives. Recent applications of such technique to INS can be found in [8], [9] where vision-aided UAVs are considered (the latter exploiting a diffeomorphism to simplify the analysis).

The aforementioned frameworks focus on instantaneous/local observability. Studies concerning global properties have been presented in [10], [11], [12]. However, less rigorous evaluations are performed, differentiating the measurements function (w.r.t. time) and considering particular scenarios to draw analytical conclusions about system observability in those situations. For instance, [11] and [12] provide conditions for trajectories with static/constant-attitude periods and phases with non-zero angular velocity. In [13], [14] a thoughtful observability analysis is presented for the case of vision-assisted INS. The concept of indistinguishable states from the available measurements is exploited to prove that, when sensor biases dynamics are not assumed noise-independent from the other states, the indistinguishable set is not a singleton, i.e. the system is not observable. In addition, bounds are given on the volume of such set.

In this work we make use of indistinguishable trajectories as well, to characterize global observability for the case of UAVs equipped with a standard aided-INS unit (exploiting GNSS) and a visual odometry system (like the one proposed in [15]) providing information about velocity w.r.t. the inertial frame, expressed in body coordinates. In this context, it is required to achieve attitude estimation, as well as accelerometer and gyro bias compensation. The aim is to provide explicit conditions for trajectories indistinguishability showing how, by means of a suitable change of coordinates (exploited solely for analysis purposes), velocity information given by the visual system allows to enhance observability of attitude and biases. From a theoretical viewpoint, our approach differs from [13], [14] in that we represent the set of indistinguishable states as the solutions of Differential Algebraic Equations. A similar approach is exploited in [16] for the case of induction motors. Moreover, to specialize the analysis to significant cases usually encountered in real-

A. Bosso, N. Mimmo, C. Conficoni and A. Tilli are with the Center of Complex Automated Systems (CASY) at the Department of Electrical, Electronic and Information Engineering (DEI), University of Bologna, Viale Risorgimento, 2, 40136 Bologna, Italy. {alessandro.bosso3,nicola.mimmo, christian.conficoni3, andrea.tilli}@unibo.it

world applications, we provide explicit conditions in terms of system inputs (cf. [17], where a simplified scenario dealing with linear motion quantities is treated). In particular, similarly to the Adaptive Systems framework, we cast observability in terms of *Persistency of Excitation* conditions. From a practical point of view, this gives a profitable way to understand which kind of maneuvers are needed to ensure state reconstruction.

The paper is organized as follows. In section II the kinematic model is introduced, together with the equations for IMU sensors, GNSS position measures and visual odometry. Section III is the core of this work, containing the observability analysis and characterizing, after a proper statement of the problem, the INS indistinguishable dynamics. In Section IV, simulation tests concerning the aforementioned UAV application (with a standard EKF as state observer) are provided to validate the theoretical results. Section V wraps up the paper with final considerations and remarks.

NOTATION

Throughout this work, we denote with $SO(n)$ and $\mathfrak{so}(n)$ the special orthogonal group of dimension n and its Lie algebra, respectively. We use $\mathcal{S}^1$ to refer to the unitary circle, which is an equivalent representation of $SO(2)$. Operator $S(\cdot)$ is used to denote skew-symmetric matrices, in particular:

$$S(a) = \begin{bmatrix} 0 & -a \\ a & 0 \end{bmatrix} \in \mathfrak{so}(2) \qquad a \in \mathbb{R}$$

$$S\left(\begin{bmatrix} a_x \\ a_y \\ a_z \end{bmatrix}\right) = \begin{bmatrix} 0 & -a_z & a_y \\ a_z & 0 & -a_x \\ -a_y & a_x & 0 \end{bmatrix} \in \mathfrak{so}(3) \qquad \begin{bmatrix} a_x \\ a_y \\ a_z \end{bmatrix} \in \mathbb{R}^3$$

The notation is the same in both cases because the meaning is clear from the context. We use $\text{vex}(\cdot) : \mathfrak{so}(3) \to \mathbb{R}^3$ to denote the inverse operator of $S(\cdot)$ in dimension 3. Finally, I_n represents the identity matrix of dimension n.

II. KINEMATIC AND SENSOR MODELS

A. Kinematic Equations

Let us consider, for the purpose of our analysis, the kinematic model of a rigid body moving in an inertial reference frame. The state space representation of the system can be described as follows [1]:

$$\begin{aligned} \dot{p}^n &= R_{nb} v^b \\ \dot{v}^b &= u^b - S(\omega_{nb}^b) v^b \\ \dot{R}_{nb} &= R_{nb} S(\omega_{nb}^b), \end{aligned} \tag{1}$$

where p^n is the position in the navigation frame (we adopt ENU convention), v^b is the navigation velocity, represented in the body frame, and R_{nb} is the attitude between the two reference frames, while u^b and and ω_{nb}^b are the total acceleration and body angular velocity, respectively, represented in the body frame. We will avoid, in order to show more effectively the structural properties of the model, to introduce the non ideal effects of a navigation in a non-inertial frame of reference. However, the properties that arise in the inertial case could be extended to the more general framework in a similar fashion, accounting for the coupling effects that arise in that scenario. The mathematical models related to the sensors of choice are now presented.

B. Inertial Measurement Unit

We consider a typical strap-down IMU based on MEMS technologies, equipped with accelerometer and rate gyro sensors. Magnetometer readings, usually available in commercial IMUs, are not used so as to attain a more robust set of measurements: magnetometers can, in fact, be heavily affected by the disturbances caused by nearby machinery or the electric motors on board the UAV.

For a strap-down device, the retrieved values are given in a reference frame with constant relative rotation w.r.t. vehicle body axes[1]. Indeed, for the purpose of this work, it is assumed that body and measurement frames are coincident: the angular alignment errors can be removed with an offline calibration of the platform. The accelerometer and gyro readings are, respectively:

$$\begin{aligned} u_s &= u^b - R_{bn} g + \tilde{u} \\ \omega_s &= \omega_{nb}^b + \tilde{\omega}. \end{aligned} \tag{2}$$

The variables $\tilde{u}$ and $\tilde{\omega}$ are sensor errors, and are indeed stochastic processes. Vector g is the local gravity vector, represented in the navigation frame of reference, and is assumed, in this work, known and constant (e.g., in typical applications close to the surface of the Earth, $g \simeq [0 \;\; 0 \;\; -9.81]^T$). In particular, we can separate each process into white and colored noise:

$$\begin{aligned} \tilde{u} &= b_u + w_u \\ \tilde{\omega} &= b_\omega + w_\omega, \end{aligned} \tag{3}$$

where w refers to the white part and b, on the other hand, to the correlated part, which is usually referred to as bias, or pseudo-bias. Even though it is common practice to regard b_u and b_ω as constant (or slowly varying) parameters, these variables cannot be effectively estimated offline due to their high dependance on drifts and device temperature, which causes them to slowly change during operation time: their online estimation is therefore a crucial element for quality inertial navigation, in particular when using low-cost commercial IMUs.

A popular approach to modeling these biases, for observation/identification purposes, is to consider them the output of a random walk, or a stationary Gauss-Markov process with known, typically large, time constant. Although a more specific model could be adopted, in this work the random walk formulation is chosen for simplicity:

$$\begin{aligned} \dot{b}_u &= \nu_u \\ \dot{b}_\omega &= \nu_\omega, \end{aligned} \tag{4}$$

where ν_u and ν_ω are zero-mean Gaussian white noises, with known variances.

C. Exteroceptive Sensors

In this work, we consider two specific exteroceptive measurements, a GNSS/Indoor position sensor and vision-based

[1]We are neglecting the effects due to the lever arm, and the possible mechanical vibrations induced between IMU and vehicle.

odometry. For what concerns GNSS/Indoor position information, the following model is considered:

$$p_s = p^n + n_p, \tag{5}$$

where n_p is a white noise[2].

Finally, the visual odometry device that is considered in this work is an optical flow sensor with the capability of providing velocity measurement in three orthogonal axes. Since nowadays CMOS optical flow sensors are equipped with a sonar sensor that rescales flow in a metric value and a gyroscope that compensates body rotation [15], the output of the device is navigation velocity, expressed in the body frame of reference:

$$v_s = v^b + n_v. \tag{6}$$

III. Observability Analysis based on Indistinguishable Dynamics

In this section, the observability analysis for inertial navigation with visual odometry is presented. Firstly, a general theoretical framework is provided, introducing a particular definition of observability which will be of crucial importance for the next results. Following that, the main result is presented, together with the in-depth analysis of a special case that often occurs in practical applications.

A. Problem Statement

Recall the state space representation of non-linear systems:

$$\begin{aligned} \dot{x} &= f(x,u) \\ y &= h(x), \end{aligned} \tag{7}$$

where $x \in \mathcal{X} \subset \mathbb{R}^n$ ($\mathcal{X}$ a $\mathcal{C}^\infty$connected manifold), $u \in \mathbb{R}^m$ and $y \in \mathbb{R}^p$. Let $\|\cdot\|_{\mathcal{X}}$ be a distance on $\mathcal{X}$. Assume f is Lipschitz continuous, so that existence and uniqueness of solutions is guaranteed, and assume h sufficiently smooth. Consider $u(\cdot) \in \mathcal{U}$, where $\mathcal{U}$ is a set of functions in $\mathbb{R}^m$ defined on $[t_0,\ +\infty)$. Denote with $x(x_0, u(\cdot), t)$ the solution of the above system, evaluated at time t, with initial condition x_0 (at time t_0) and input sequence $u(\cdot)$. Without loss of generality, consider $t_0 = 0$. Exploiting these elements, the following definitions of indistinguishability, observability and detectability are provided [16].

Definition 1 ($u(\cdot)$-*Indistinguishability*): Let x_1, x_2 in $\mathcal{X}$. Let $u(\cdot) \in \mathcal{U}$. Then x_1 and x_2 are called $u(\cdot)$-*Indistinguishable* in the interval $[0,\ T)$ if, $\forall t \in [0,\ T)$, $h(x(x_1, u(\cdot), t)) = h(x(x_2, u(\cdot), t))$.

Note that indistinguishable points in the interval $[0,\ +\infty)$ represent an equivalence class, denoted with $\mathcal{I}(x,u)$. We exploit this notation for the following definitions.

Definition 2 (*Observability*): A state x is *observable* if, for all $u(\cdot) \in \mathcal{U}$, $\mathcal{I}(x,u) = \{x\}$.

Definition 3 (*Detectability*): A state x is *detectable* if, for all $u(\cdot) \in \mathcal{U}$,

$$x' \in \mathcal{I}(x,u) \implies \lim_{t \to +\infty} \|x(x', u(\cdot), t) - x(x, u(\cdot), t)\|_{\mathcal{X}} = 0.$$

[2]Notice that in practice GNSS error is correlated with its past, because the output of the sensor is typically the state of a Kalman filter, or another estimation technique from a set of pseudo-ranges.

Clearly, the above definitions of *observability* and *detectability* extend to system (7) when they hold for all $x \in \mathcal{X}$. Furthermore, the *local* equivalent of these properties holds if the conditions above are verified in an open neighborhood N_x of x. We refer to [16] for equivalent formulations (cf. *weak observability* in [7]).

Even though the above definitions can be exploited to effectively address most observability results, a similar locality concept w.r.t the set $\mathcal{U}$ is not clearly specified. The point is, in fact, that the models that arise in inertial navigation are typically tightly coupled with input trajectories, especially when considering output function h. Taking this into account, observability/detectability properties will usually hold only within a particular subset of the input signals space. Let $\mathcal{V} \subset \mathcal{U}$. All previous definitions can be immediately "restricted" to $\mathcal{V}$, and they are denoted with $\mathcal{V}$-*observability* (*detectability*).

Taking advantage of the previous discussion, it is easy to see that global observability analysis can be recast into the study of the indistinguishable dynamics of (7), i.e. the set of all trajectories s.t. $x_0 = x(t_0) \in \mathcal{I}(x,u)$, for $x \in \mathcal{X}$ and $u \in \mathcal{V}$. In particular, if such dynamics coincides with a single trajectory, x_0 is (*locally*) $\mathcal{V}$-*observable*; if it is convergent[3] w.r.t. a single trajectory, it is (*locally*) $\mathcal{V}$-*detectable*. Constructively, the indistinguishable dynamics is based on the cascade of reference system (7) and an error model w.r.t. a second instance of the same model, possibly with different initial conditions: the set of indistinguishable states, in the interval $[0,\ T)$, is thus given by all initial conditions of the error model which have a solution over $[0,\ T)$, under the constraint that the sequence $\{h(\cdot),\ (d/dt)h(\cdot),\ \ldots\}$ coincides between the two instances of (7), $\forall t \in [0,\ T)$.

B. The Inertial Navigation Indistinguishable Dynamics

We begin by introducing the model for aided-INS in original and error coordinates. Exploiting (1)-(2), and discarding the explicit frame reference for compactness of notation ($R = R_{nb}$), we obtain the following navigation equations:

$$\boldsymbol{\Sigma}: \begin{cases} \dot{p} = Rv \\ \dot{v} = (u_s - \tilde{u}) + R^T g - S(\omega_s - \tilde{\omega})v \\ \dot{R} = RS(\omega_s - \tilde{\omega}) \\ \dot{\tilde{u}} = \gamma_u \\ \dot{\tilde{\omega}} = \gamma_\omega \end{cases}, \tag{8}$$

where $\tilde{u}$ and $\tilde{\omega}$ are regarded as states, with derivatives γ_u and γ_ω which will be specified in the following, and u_s, ω_s treated as system inputs. We assume $u_s - \tilde{u}$, $\omega_s - \tilde{\omega}$ bounded. In order to proceed with the observability analysis, all white noises, which bring no useful information for the observation, are discarded from the model. Introducing a second instance of model (8), denoted as $\boldsymbol{\Sigma}_2$ (with states p_2, v_2, R_2, b_{u2} and $b_{\omega 2}$), and defining the error coordinates as $\tilde{p} = p - p_2$, $\tilde{v} = v - v_2$, $\tilde{R} = R_2^T R$, $\tilde{b}_u = b_u - b_{u2}$ and $\tilde{b}_\omega = b_\omega - b_{\omega 2}$, the resulting error dynamics between $\boldsymbol{\Sigma}$ and

[3]Note that, with the above definitions, asymptotic stability is not required.

$\mathbf{\Sigma}_2$, under the same inputs u_s, ω_s, becomes:

$$\mathbf{\Sigma}_e : \begin{cases} \dot{\tilde{p}} = R(I_3 - \tilde{R})^T v + R\tilde{R}^T \tilde{v} \\ \dot{\tilde{v}} = -\tilde{b}_u + (I_3 - \tilde{R})R^T g - S(\omega_s - b_\omega)\tilde{v} + S(\tilde{b}_\omega)(v - \tilde{v}) \\ \dot{\tilde{R}} = \tilde{R}S(\omega_s - b_\omega) - S(\omega_s - b_\omega)\tilde{R} - S(\tilde{b}_\omega)\tilde{R} \\ \dot{\tilde{b}}_u = 0 \\ \dot{\tilde{b}}_\omega = 0 \end{cases} \tag{9}$$

where the identity $d(R^T)/dt = -R^T \dot{R} R^T$ was exploited to obtain the attitude error dynamics. Throughout all the paper, the following output function is adopted:

$$y = \begin{bmatrix} p \\ v \end{bmatrix}. \tag{10}$$

The first important result of this work is now presented.

Lemma 1 (*Inertial Navigation Indistinguishable Dynamics - non-zero speed*): Assume $v(t) \neq 0$ for $t \in [0,\ T)$, then the indistinguishable dynamics of system $\mathbf{\Sigma}$ in $[0,\ T)$, with output function (10), is given by the cascade of $\mathbf{\Sigma}$ and the following DAE on a manifold of dimension 2:

$$\mathbf{\Sigma}_i : \begin{cases} \dot{\zeta} = -S(b)\zeta \\ \dot{b} = -\begin{bmatrix} 0_{1\times 2} & \bar{\omega}_{\hat{v}}^T \end{bmatrix} \beta \\ \dot{\beta} = -\operatorname{diag}\{S(\omega_{x\hat{v}}),\ S(\omega_{x\hat{v}})\}\beta + \begin{bmatrix} 0_{2\times 1} \\ \bar{\omega}_{\hat{v}} \end{bmatrix} b\,, \\ \beta = \Psi\left(\zeta - \begin{bmatrix} 1 \\ 0 \end{bmatrix}\right) \end{cases} \tag{11}$$

where $\zeta = [\cos(\phi)\ \sin(\phi)]^T \in \mathcal{S}^1$ is the angular error about the point-wise direction of vector v, $\beta = [\tilde{b}'_{uy}\ \tilde{b}'_{uz}\ \tilde{b}'_{\omega z}\ -\tilde{b}'_{\omega y}]^T$, $b = \tilde{b}'_{\omega x}$, $\tilde{b}'^T_u = [\tilde{b}'_{ux}\ \tilde{b}'_{uy}\ \tilde{b}'_{uz}] = (C^T\tilde{b}_u)^T$, $\tilde{b}'^T_\omega = [\tilde{b}'_{\omega x}\ \tilde{b}'_{\omega y}\ \tilde{b}'_{\omega z}] = (C^T\tilde{b}_\omega)^T$, while $C \in SO(3)$ is such that $(C^T v)^T = [v'_x\ 0\ 0]$. Finally, $\dot{C} = C\Omega_{\hat{v}}$, $[\omega_{x\hat{v}}\ \bar{\omega}_{\hat{v}}^T]^T = \operatorname{vex}(\Omega_{\hat{v}})$ and:

$$\Psi = \begin{bmatrix} \bar{u}' & S(1)\bar{u}' \\ \bar{\omega}' & S(1)\bar{\omega}' \end{bmatrix} = \begin{bmatrix} U \\ \Omega \end{bmatrix},$$

with $\bar{u}' = [u'_y\ u'_z]^T$, $\bar{\omega}' = [\omega'_z\ \ -\omega'_y]^T$, $[u'_x\ u'_y\ u'_z] = (C^T(u_s - b_u))^T$ and $\omega'^T = [\omega'_x\ \omega'_y\ \omega'_z] = (C^T(\omega_s - b_\omega) + \operatorname{vex}(\Omega_{\hat{v}}))^T$.

Proof: To enforce indistinguishability between $\mathbf{\Sigma}$ and $\mathbf{\Sigma}_2$, let $\tilde{p}(t) = 0$, $\tilde{v}(t) = 0$ for all t in $[0\ T)$, hence all derivatives are zero. Exploiting the position equation of $\mathbf{\Sigma}_e$:

$$(I_3 - \tilde{R})^T v = 0 \iff C^T(I_3 - \tilde{R}^T)C \begin{bmatrix} v'_x \\ 0 \\ 0 \end{bmatrix} = 0.$$

Denoting $\tilde{R}' = C^T\tilde{R}C$, note that the above equation implies the first row of $\tilde{R}'$ is $[1\ 0\ 0]$, which, by orthogonality, yields:

$$\tilde{R}' = \begin{bmatrix} 1 & 0_{1\times 2} \\ 0_{2\times 1} & \tilde{r}' \end{bmatrix}, \tag{12}$$

where $\tilde{r}' \in SO(2)$ is a planar rotation matrix. Intuitively, this rotation represents an unknown error rotation about the measured velocity, which is however time-varying in the body reference frame. Because of the misalignment between body axes and velocity vector, the rotation matrix C is introduced in order to restore alignment. C is known in the body frame of both $\mathbf{\Sigma}$ and $\mathbf{\Sigma}_2$ because it holds that:

$$C = \left[\tfrac{v}{|v|} \ \middle|\ (*)\right], \tag{13}$$

and $(*)$, exploited to preserve orthogonality, is chosen as a function of v. Note that there is no preferred orientation about velocity, and this leaves $\omega_{x\hat{v}}$ as a degree of freedom. The derivative of C can be chosen to be the same in both frames of reference, in fact assume that $\Omega_{1\hat{v}} \neq \Omega_{2\hat{v}}$ (the first component can be chosen equal) then:

$$\frac{d}{dt}(Cv - Cv_2) = C\dot{\tilde{v}} + C(\Omega_{1\hat{v}} - \Omega_{2\hat{v}})v = 0,$$

because $C(t)\tilde{v}(t)$ is 0 for all t, then the assumption is false for any $v \neq 0$. Consequently, the velocity and attitude equations of $\mathbf{\Sigma}_e$ are thus reformulated:

$$\begin{aligned} 0 &= -\tilde{b}'_u + (I_3 - \tilde{R}')C^T R^T g - S(\tilde{b}'_\omega) \begin{bmatrix} v'_x \\ 0 \\ 0 \end{bmatrix} \\ \dot{\tilde{R}}' &= \tilde{R}'S(\omega') - S(\omega')\tilde{R}' - S(\tilde{b}'_\omega)\tilde{R}' \end{aligned} \tag{14}$$

The next part of the proof consists of a direct substitution of (12) into (14). First of all, note that the first equation ensures $\tilde{b}'_{ux} = 0$, while the remaining two components can be arranged as:

$$-\bar{b}'_u + \bar{g}' - \tilde{r}'\bar{g}' + \bar{b}'_\omega v'_x = 0,$$

where $\bar{g}' = [g'_y\ g'_z]^T$, $[g'_x\ g'_y\ g'_z]^T = C^T R^T g$ and $\bar{b}'_u = [\tilde{b}'_{uy}\ \tilde{b}'_{uz}]^T$, $\bar{b}'_\omega = [\tilde{b}'_{\omega z}\ \ -\tilde{b}'_{\omega y}]^T$. For what concerns the attitude equation, in a similar fashion a differential and an algebraic equation are obtained:

$$\begin{aligned} \dot{\tilde{r}}' &= -S(b)\tilde{r}' \\ \tilde{r}'\bar{\omega}' - \bar{\omega}' - \bar{b}'_\omega &= 0. \end{aligned}$$

Moreover, the same procedure can be applied to velocity dynamics of system $\mathbf{\Sigma}$:

$$\begin{aligned} \dot{v}'_x &= u'_x + g'_x \\ \bar{u}' + \bar{g}' - \bar{\omega}' v'_x &= 0, \end{aligned} \tag{15}$$

therefore:

$$\begin{aligned} \dot{\tilde{r}}' &= -S(b)\tilde{r}' \\ (\tilde{r}' - I_2)\bar{\omega}' &= \bar{b}'_\omega \\ (\tilde{r}' - I_2)\bar{u}' &= \bar{b}'_u. \end{aligned}$$

Finally, let ϕ s.t.:

$$\tilde{r}' = \begin{bmatrix} \cos(\phi) & -\sin(\phi) \\ \sin(\phi) & \cos(\phi) \end{bmatrix},$$

this way it is possible to apply the change of coordinates from $\tilde{r}'$ to ζ. At last, computing the derivatives of the new biases, the statement follows directly. □

Remark 1: Note that the indistinguishable dynamics is associated to time-varying directions w.r.t. body axes. This means that, intuitively, a way to ensure observability of the whole state is to enforce sufficient excitation in order to make all body axes, during "frequent enough" time intervals, incompatible with a non-trivial solution of $\mathbf{\Sigma}_i$. Clearly, this

is close to the idea of *Persistency of Excitation* from the fields of System Identification and Adaptive Control.

***Remark** 2:* C is not necessary for the purpose of observer design, it is mainly an analysis tool. Moreover, as previously stated, $vex(\Omega_{\hat{v}})$ has degree of freedom in $\omega_{\hat{v}x}$, which can be set equal to zero to make $\bar{b}'_u$ a constant parameter, thus reducing the complexity of $\mathbf{\Sigma}_i$.

***Remark** 3:* Notice that the reformulation of reference trajectories of $\mathbf{\Sigma}$ in (15) is not a restriction of possible input sequences, indeed this constraint is a direct consequence of the choice of C.

Another important aspect of the analysis that is dealt with is the case of constantly null speed, which typically appears in practical applications (e.g. when the UAV hovers over a fixed position).

Lemma 2 (*Inertial Navigation Indistinguishable Dynamics - zero speed*): Assume $v(t) = 0$ for $t \in [0,\ T)$, then the indistinguishable dynamics of system $\mathbf{\Sigma}$ in $[0,\ T)$, with output function (10) is given by the cascade of $\mathbf{\Sigma}$ and the following DAE on a manifold of dimension 4:

$$\mathbf{\Sigma}_{i0}: \begin{cases} \dot{Z} = -S(\tilde{b}'_\omega)Z \\ \dot{\tilde{b}}'_u = -\Omega_0 \tilde{b}'_u \\ \dot{\tilde{b}}'_\omega = -\Omega_0 \tilde{b}'_\omega \\ \left(\bar{z} - \begin{bmatrix}1 & 0 & 0\end{bmatrix}^T\right) u' = \tilde{b}'_u \\ S(\tilde{b}'_\omega)\bar{z} = -\Omega_0 \left(\bar{z} - \begin{bmatrix}1 & 0 & 0\end{bmatrix}^T\right) \end{cases}, \tag{16}$$

where $Z \in SO(3)$, with $\tilde{b}'_u = C_0^T \tilde{b}_u$, $\tilde{b}'_\omega = C_0^T \tilde{b}_\omega$, C_0 s.t. $[u'\ 0\ 0]^T = C_0^T(u_s - b_u)$ and $\dot{C}_0 = C_0\Omega_0 = -C_0 S(C_0^T(\omega_s - b_\omega))$. Finally, $\bar{z}$ is the first column of Z.

Proof: We notice that speed constantly zero implies:

$$\begin{aligned} \tilde{b}_u &= (I_3 - \tilde{R})R^T g \\ R^T g &= -(u_s - b_u). \end{aligned} \tag{17}$$

The second relation can be derived to obtain a differential equation for $u'_s = u_s - b_u$ (we denote $\omega'_s = \omega_s - b_\omega$):

$$\dot{u}'_s = R^T \dot{R} R^T g = S(\omega'_s)R^T g = -S(\omega'_s)u'_s,$$

which states the clear fact that the only variation of measured forces is due to the change of gravity orientation. Taking now the derivative of the first equation:

$$\dot{\tilde{R}}u'_s - (\tilde{R} - I_3)S(\omega'_s)u'_s = 0. \tag{18}$$

Similarly to the Lemma 1, the choice of C_0 leaves one degree of freedom, i.e. the angle about the known vector axis, which in this case is that of gravity. Since $C_0^T u'_s$ is obviously constant (its amplitude coincides with that of g, and its orientation is fixed), we have that:

$$\Omega_0 C_0^T u'_s + C_0^T S(\omega'_s)u'_s = 0.$$

W.l.o.g., we select $\text{vex}(\Omega_0) = -C_0^T \omega'_s$. Indeed, the only unconstrained component of angular velocity $vex(\Omega_0)$, from the above equation, is the first one, which can be chosen arbitrarily. The attitude equation is therefore simplified with $Z = C_0^T \tilde{R} C_0$:

$$\dot{Z} = -S(\tilde{b}'_\omega)Z. \tag{19}$$

To complete the proof, expanding the expression of $\dot{\tilde{R}}$ in (18) and exploiting (17) yields the algebraic equations of $\mathbf{\Sigma}_{i0}$. □

Clearly, $\mathbf{\Sigma}_i$ and $\mathbf{\Sigma}_{i0}$ can combined in order to describe thoroughly the structure of the indistinguishable dynamics. A possible approach to deal with the different DAEs according to the current state of body speed, is to exploit a hybrid formulation. The following theorem, which summarizes the previous results, goes exactly in this direction, and can be regarded as the main result of this work.

***Theorem** 1:* The indistinguishable trajectories of system $\mathbf{\Sigma}$ are entirely characterized by the cascade of system $\mathbf{\Sigma}$ and the solutions to the following system:

$$\mathcal{H}_i = \begin{cases} \dot{z} = f_q(z, u_s - b_u, \omega_s - b_\omega) & (z,q) \in C \\ \dot{q} = 0 & \\ z^+ \in \text{Proj}_{1-q}(z) & (z,q) \in D, \\ q^+ = 1 - q & \end{cases} \tag{20}$$

where $C = \mathcal{M}(f_q) \times \{q\ s.t.\ q = \text{sgn}(\max\{|v|,\ |\dot{v}|\})\}$, $D = \mathcal{M}(f_q) \times \{q\ s.t.\ q \neq \text{sgn}(\max\{|v|,\ |\dot{v}|\})\}$, $C, D \subset \mathbb{R}^6 \times SO(3) \times \mathbb{R}^6 \times \{0,1\}$, f_q and $\mathcal{M}(f_q)$ are, respectively, the flow and the domain manifold of the DAEs ($\mathbf{\Sigma}_{i0}$ for $q = 0$ and $\mathbf{\Sigma}_i$ for $q = 1$), while $\text{Proj}_{1-q}(\cdot)$ is a projection operator which maps the current state z to the set of points with null distance from it in $\mathcal{M}(f_{1-q})$.

Proof: The result follows directly from Lemma 1 and Lemma 2. Note that in case $|v(t)| = 0$ and $|\dot{v}(t)| \neq 0$, then no transition from $\mathbf{\Sigma}_i$ to $\mathbf{\Sigma}_{i0}$ can occur because there exists an open interval containing t where the set $\{t'\ s.t.\ |v| = 0\}$, also due to $\mathbf{\Sigma}$ being Lipschitz continuous and the inputs bounded, is not Lebesgue measurable. □

***Remark** 4:* Even if the error system $\mathbf{\Sigma}_e$, which contains the trajectories of both $\mathbf{\Sigma}_i$ and $\mathbf{\Sigma}_{i0}$, is Lipschitz continuous, the jump map of $\mathcal{H}_i$ is possibly a point-to-set map. Indeed, it may happen that $z^+ \in \emptyset$ depending on the considered trajectory.

***Remark** 5:* Since the solutions $\mathcal{H}_i$ are not necessarily complete, a constructive algorithm to "rule out" initial conditions that are not indistinguishable could be obtained, dedicating particular attention to the effect of jumps[4].

***Remark** 6:* The condition on $|v|$ and $|\dot{v}|$ explained above, apart from being a technical requirement to avoid introducing a third case, can be useful to exclude *Zeno* arcs. However, it is possible to approximate $\mathcal{H}_i$ with a hysteresis mechanism to switch between the two modes: this can be used to deal with disturbances and model mismatch.

The reduced model that was presented represents a powerful tool that can be used for both synthesis and analysis. Firstly, we infer that $\mathbf{\Sigma}$ is not observable, not detectable, not locally observable, not locally detectable. In the following, to conclude with a derivation of the previous results, we show a set of sufficient conditions for local $\mathcal{V}$-observability, which covers a large amount of significant trajectories for practical applications. The general case, whose analysis would be significantly more technical, is not treated for simplicity.

[4]For brevity, this specific part will not be dealt with in this paper. However, an interesting intuition is that jumps from $\mathbf{\Sigma}_{i0}$ to $\mathbf{\Sigma}_i$ are associated with a reduction in the domain dimension.

Proposition 1 (*Observability for constant velocity direction*): Assume $v(t) \neq 0$, $\forall t$ and $C_{\hat{v}}$ (s.t. $C_{\hat{v}}^T v = [v'_x \ 0 \ 0]^T$) is constant. Consider system $\mathbf{\Sigma}_i$, then if $|\bar{\omega}'| \neq 0$ or $|\bar{u}'| \neq 0$ and one of the following conditions is satisfied ($e_1 = [1 \ 0]^T$):

1) Ψ is such that either Ω or U is constant, non zero, and the following *Persistency of Excitation* (*PE*) condition is satisfied for U (resp. for Ω):
$$\exists \alpha_1, \ \alpha_2, \ T_0 \ s.t. \ \alpha_1 I_2 \leq \int_t^{t+T_0} \dot{U}^T(\tau)\dot{U}(\tau)d\tau \leq \alpha_2 I_2, \tag{21}$$
for all $t \geq t_0$, with $\alpha_1 > 0$, $\alpha_2 > 0$ and $T_0 > 0$;
2) Ψ is such that either Ω or U is zero, and the following PE condition is satisfied for U (resp. for Ω):
$$\exists \alpha_1, \ \alpha_2, \ T_0 \ s.t. \ \alpha_1 I_3 \leq \int_t^{t+T_0} \Phi_U(\tau)\Phi_U^T(\tau)d\tau \leq \alpha_2 I_3, \tag{22}$$
for all $t \geq t_0$, with $\alpha_1 > 0$, $\alpha_2 > 0$ and $T_0 > 0$, and $\Phi_U^T = [\ddot{U}U^{-1} - \dot{U}U^{-1}\dot{U}U^{-1} \ \big| \ -S(1)\dot{U}e_1]$ (the same structure is for Φ_Ω);
3) Ψ is such that Ω, U are non zero and the following *PE* condition is satisfied:
$$\exists \alpha_1, \ \alpha_2, \ T_0 \ s.t.$$
$$\alpha_1 I_2 \leq \max_{Y \in \{U, \ \Omega\}} \int_t^{t+T_0} \Gamma_Y(\tau)\Gamma_Y^T(\tau)d\tau \leq \alpha_2 I_2, \tag{23}$$
for all $t \geq t_0$, with $\alpha_1 > 0$, $\alpha_2 > 0$ and $T_0 > 0$, and Γ_Y^T, $Y \in \{U, \ \Omega\}$, defined as $[U^{-1}\dot{U} - \Omega^{-1}\dot{\Omega}]Y^{-1}$;
4) alternatively to *PE* conditions 2-3, for either U or Ω, the matrix in (22) is diagonal, and (21) is satisfied;

then system $\mathbf{\Sigma}$ is *locally-$\mathcal{V}$-observable*, with open neighborhood chosen as the open set s.t. $v \neq 0$, and $\mathcal{V}$ equal to the set of trajectories s.t. the above conditions hold. Furthermore, if both Ω and U are constant and non zero, then ζ is a constant error and $b = 0$, but β is completely unknown. If either Ω or U is non zero and constant, and U (resp. Ω) is zero, then $\bar{b}'_u = 0$ (resp. $\bar{b}'_\omega = 0$), $b = 0$, ζ is constant and $\bar{b}'_\omega$ (resp. $\bar{b}'_u$) is unknown. If both Ω and U are zero, $\beta = 0$ and ζ, b are completely unknown.

Proof: Condition 1 can be trivially verified considering that if Ω or U is constant and non-singular, ζ is constant, thus $b = 0$ and therefore if $\bar{b}'_u = 0$ or $\bar{b}'_\omega = 0$, then all other variables are so. Note that *PE* condition (21) is stronger than simply enforcing the derivative different from zero. For what concerns condition (2), the issue is that we cannot implicitly infer ζ constant and $b = 0$. Taking the derivative of $U(\zeta - e_1)$ (the computations are equivalent for the case of Ω):
$$\dot{U}(\zeta - e_1) - US(b)\zeta = 0.$$
Because U and $S(b)$ commute (U is a rotation matrix rescaled by $|u|$), we have that:
$$\dot{U}(\zeta - e_1) - S(b)\underbrace{U(\zeta - e_1)}_{\bar{b}_u} - S(b)Ue_1 = 0.$$
Computing again the derivative, and noticing that $(d/dt)(\zeta - e_1) = -U^{-1}\dot{U}(\zeta - e_1)$:
$$\ddot{U}U^{-1}\bar{b}'_u - \dot{U}U^{-1}\dot{U}U^{-1}\bar{b}'_u - S(1)\dot{U}e_1 b = 0, \tag{24}$$
from which the second *PE* condition (22) follows directly. To prove (23), it is sufficient to note that, taking the derivative of $U(\zeta - e_1)$ and $\Omega(\zeta - e_1)$, we have $[U^{-1}\dot{U} - \Omega^{-1}\dot{\Omega}](\zeta - e_1) = 0$. Condition 4, instead, easily implies $b = 0$, ζ constant, and therefore case (1) is restored. The cases of indistinguishability that were listed are trivially verified by direct substitution. □

***Remark** 7:* The above scenario, even if restricted to constant velocity directions in the body frame, is a situation that often occurs in practical situations, so the *PE* conditions that have been stated are crucial for observer design.

***Remark** 8:* It is possible to extend the framework to non-constant velocity orientation[5]. In that case, more coupling between signals is expected because of the presence of $\Omega_{\hat{v}}$ in the dynamics of $\bar{b}'_u$ and $\bar{b}'_\omega$. Intuitively, similar conditions could be carried out to express how maneuvering of the vehicle can enforce observability.

To conclude this section, a simple example is presented.

Example 1 (*Circular motion*): Consider a vehicle in circular motion, with fixed body velocity direction (w.l.o.g., assume $v^b = [V \ 0 \ 0]^T$), then it is easy to see that, in the absence of *roll* maneuvers (about velocity), inputs do not satisfy *PE* condition (22). According to Proposition 1, *$\mathcal{V}$-observability* can be achieved with a *roll* rotation (ω^b_{nbx}), thus satisfying either condition 4, if vertical speed $\omega^n_{nbz} = const$ (planar circular motion), or condition 3, if $\omega^b_{nbz} = const$. With a similar strategy, it is possible to prove observability for a large amount of trajectories, e.g. wavy lines, spirals or helicoidal trajectories. The same arguments can be extended to compositions of trajectories, where $\mathcal{H}_i$ can be exploited to make the analysis of complex segments treatable, and therefore establish observability even if some of them do not satisfy *PE* conditions, or their behavior is unknown.

IV. Simulation Results

This section presents a set of simulation tests performed to validate the indistinguishability conditions previously found. The simulator, written in Matlab/Simulink, implements the dynamics of a quad-copter equipped with an IMU (with gyro and accelerometer) a GPS receiver for North-East position feedback, a range finder which retrieves terrain relative altitude, and an optical flow sensor. The drone model is comprehensive of a standard guidance and stabilization system (nested PIDs), that represents the typical control strategy for this kind of application.

An Extended Kalman Filter is implemented as benchmark for the simulations: it is chosen, with the purpose of showing more evidently the observability properties, to exploit a hybrid structure, with continuous-time predictor and discrete events for correction (sample time $0.1s$), instead of a fully discrete-time version that would introduce non-idealities due to approximation of the differential equation. All algorithms are implemented using the quaternion representation, however the results will be shown with the Euler's angles, denoting with φ, ϑ and ψ *roll*, *pitch* and *yaw*, respectively.

[5]This analysis is out of the purpose of this work.

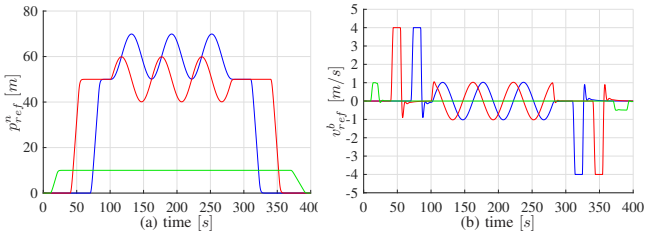

Fig. 1. (a): reference positions $p^n_{ref,x}$ (blue), $p^n_{ref,y}$ (red) and $p^n_{ref,z}$ (green) for the considered mission. (b): resulting velocity profile in the absence of wind turbulence with $v^n_{ref,x}$ (blue), $v^n_{ref,y}$ (red) and $v^n_{ref,z}$ (green).

In the following, as a case of study, we will exploit a mission composed of several operating conditions, firstly in completely ideal and then in noisy/windy conditions. For what concerns the mission profile, the quad-copter starts at rest on the ground and, after the takeoff, it is called to reach a series of way-points with an intermediate loiter phase. In Figure 1, reference position and the resulting reference velocity in absence of wind are depicted. More in detail, the various steps of the maneuver are the following:

1) $t = 0$s (static on ground): the quad-copter stands at $p^n = [0\ 0\ 0]^T m$. In this scenario system $\mathbf{\Sigma}_{i0}$, with $vex(\Omega_0) = 0$, holds. In particular, according to the resulting DAE structure, all bias errors are constant, whereas the error matrix Z has one degree of freedom. It is interesting to notice that $\bar{z}$ is constant, thus the only remaining dynamic equation is a constant rotation about that vector. To confirm this behavior, it is possible to appreciate in Fig. 2 an evident drift of $\tilde{\psi}$ in this part (there is a small variation of the other components as well, because the error axis depends on the initialization), while all biases are slowly varying and converging to constant values. Note that, because the initial attitude error is small, according to $\mathbf{\Sigma}_{i0}$, $\tilde{b}_{uz}$, $\tilde{b}_{\omega x}$ and $\tilde{b}_{\omega y}$ are close to zero;
2) $t = 10s$ (take off): the quad-copter takes off and reaches a way-point at $p^n = [0\ 0\ 10]^T m$. During the take off the inertial velocity is aligned with the gravity, therefore, according to Proposition 1 (with $\Psi = 0$, $vex(\Omega_{\hat{v}}) = 0$), the yaw angle is indistinguishable together with $\tilde{b}_{\omega z}$;
3) $t = 40s$ (1st way point): the target way point is located at $p^n = [0\ 50\ 10]^T m$. The quad-copter reaches the way point along a straight path aligned with its y-body axis. In this flight condition the yaw angle is not indistinguishable any more, as well as $\tilde{b}_{\omega z}$. Because $U = const \neq 0$ in this scenario, it is possible to infer that the indistinguishable states are the accelerometer biases on the orthogonal plane w.r.t. velocity, and the angle about velocity which is constant (see Proposition 1). Due to the small roll angle, a rough approximation leads to the identification of the indistinguishable dynamics with the pitch angle, $\tilde{b}_{ux}$ and $\tilde{b}_{uz}$;
4) $t = 70s$ (2nd way point): the target way point is located at $p^n = [50\ 50\ 10]^T m$. This part of the mission shows the same results of the previous navigation branch (again recall Proposition 1) but with indistinguishable dynamics identified by the roll angle, $\tilde{b}_{uy}$ and $\tilde{b}_{uz}$;
5) $t = 100s$ (loiter): the quad-copter is called to perform a loiter around a point of interest located at $p^n = [60\ 50\ 10]^T m$. During this flight phase the drone is called to keep the heading constant, condition which guarantees that the accelerations, the angular and linear velocities are not constant and therefore, intuitively, persistently exciting. Even if not formally proved, indeed, it is possible to appreciate in Fig. 3 that this scenario ensures convergence of the observer;
6) from $t = 280s$ up to $t = 400s$ (way points to come back home): this part of the mission repeats (symmetrically) the straight paths from the base station to the initial loiter position, thus implying the same results as before.

TABLE I

NOISE CHARACTERISTICS OF THE CHOSEN SENSORS (NOISE DENSITY, STANDARD DEVIATION)

	accel. $[\frac{\mu g}{\sqrt{Hz}}]$	gyro $[\frac{deg/s}{\sqrt{Hz}}]$		GPS $[m]$	range finder $[m]$	odometry $[m/s]$
n.d.	150	0.014	st.d.	0.866	0.1	0.16

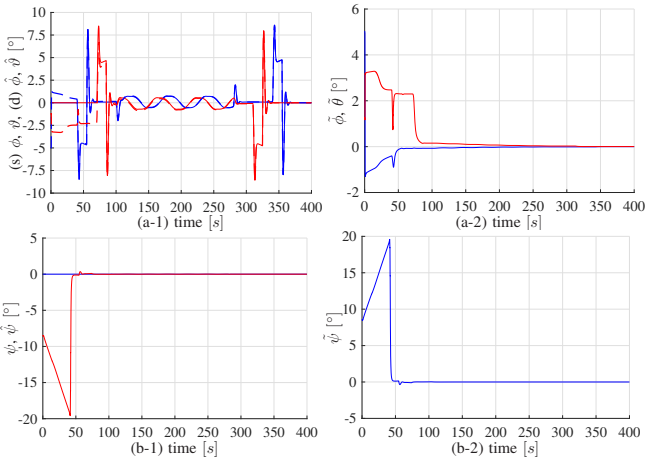

Fig. 2. Euler's angles in the ideal scenario. (a-1): roll angle (blue), pitch angle (red) and corresponding estimates. (a-2): roll (blue), pitch (red) estimation errors. (b-1): yaw (blue) and estimate (red). (b-2): yaw error. (s): solid, (d): dashed.

Furthermore, after reaching each way point and before the assignment of the new one, the quad-copter waits in hovering. This scenario, formally identical to the static condition on ground, follows the model $\mathbf{\Sigma}_{i0}$ with, in particular, $\Omega_0 = 0$. We refer to Figures 2-3 for the ideal case and Figures 4-5 for the same mission with the addition of measurement noises and wind turbulence. The noises affecting the sensors are described by their noise density (accelerometer, gyro) and by the standard deviation (GPS, range sensor, optical flow): this distinction is because the first group is affecting the flow of the hybrid implementation of the EKF, while the second is related to the jumps. Table I reports the values used throughout the simulations. The implemented wind disturbance is a Dryden model of turbulences, commonly used in aeronautical contexts, and with wind intensity (at $6m$) set to $1.5m/s$.

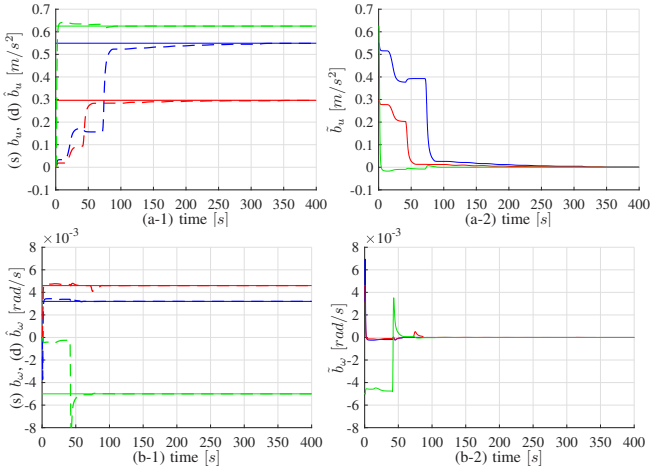

Fig. 3. Biases behavior in the ideal scenario. x component in blue, y component in red and z component in green. (a-1): accelerometer biases and their estimates. (a-2): accelerometer biases error. (b-1): gyro biases and their estimates. (b-2): gyro biases error. (s):solid. (d):dashed.

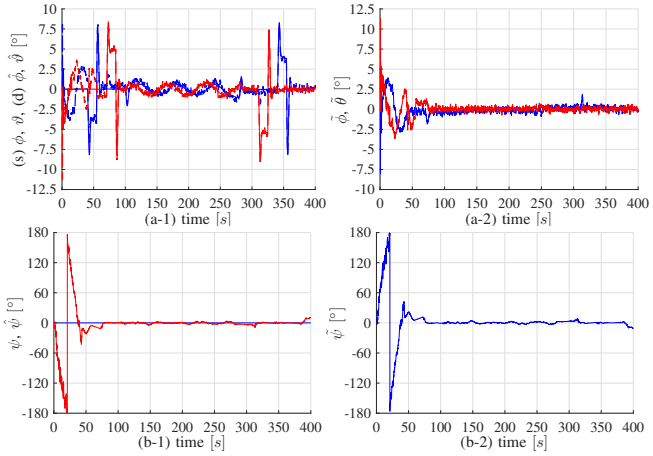

Fig. 4. Euler's angles in the noisy and windy scenario. (a-1): roll angle (blue), pitch angle (red) and corresponding estimates. (a-2): roll (blue), pitch (red) estimation errors. (b-1): yaw (blue) and estimate (red). (b-2): yaw error. (s): solid, (d): dashed.

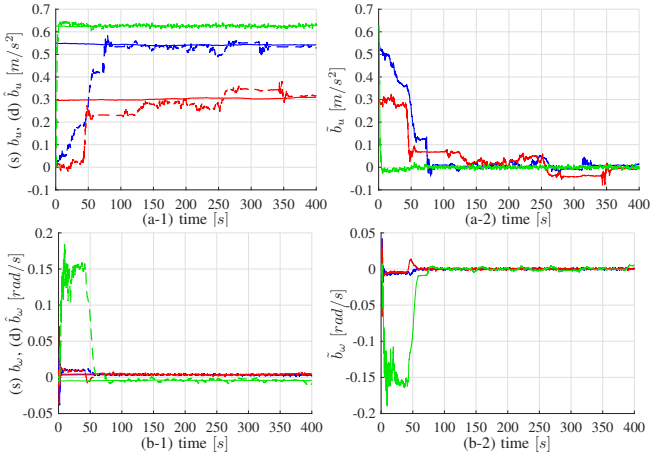

Fig. 5. Biases behavior in the noisy and windy scenario. x component in blue, y component in red and z component in green. (a-1): accelerometer biases and their estimates. (a-2): accelerometer biases error. (b-1): gyro biases and their estimates. (b-2): gyro biases error. (s):solid. (d):dashed.

V. Conclusions

This work presented a detailed global analysis concerning observability for INS with both GNSS (or equivalent position sensors) and visual odometry, which are nowadays commonly mounted on UAVs. A formal elaboration, based on the concept of indistinguishable dynamics, has led to interesting, explicit conditions on system inputs ensuring system observability and, when this is not the case, what state components can be still reconstructed and which dynamics is associated with the indistinguishable ones. Results have been specialized for working scenarios typically occurring in UAVs applications, expressing *Persistency of Excitation* conditions which can be easily exploited in practice.

Future works will be devoted to expand on such analysis, e.g. including situations where GNSS is not available, totally, or in some of its components.

References

[1] J. A. Farrell, *Aided Navigation Systems: GPS with High Rate Sensors*. McGraw Hill Professional, 2008.

[2] S. Y. Cho, B. D. Kim, Y. S. Cho, and W. S. Choi, "Observability analysis of the ins/gps navigation system on the measurements in land vehicle applications," *International Conference on Control, Automation and Systems*, pp. 841–846, 2007.

[3] S. Gao, W. Wei, Y. Zhong, and Z. Feng, "Rapid alignment method based on local observability analysis for strapdown inertial navigation system," *Acta Astronautica*, vol. 914, pp. 790–798, 2014.

[4] D. Chung and C. P. J. Lee, "Observability analysis of strapdown inertial navigation system using lyapunov transformation," *35th Conference on Decision and Control*, pp. 23–28, 1996.

[5] S. Hong, M. H. Lee, J. A. Rios, and J. Speyer, "Observability analysis of ins with a gps multi-antenna system," *KSME International Journal*, vol. 16(1), pp. 1367–1378, 2002.

[6] A. Ramanandan, A. A. Chen, and J. A. Farrell, "Real-time computer vision/dgps-aided inertial navigation system for lane-level vehicle navigation," *IEEE Trans. Intell. Transp. Syst*, vol. 13(1), pp. 235–248, 2012.

[7] R. Hermann and A. J. Krener, "Nonlinear controllability and observability," *IEEE Trans. Autom. Control*, vol. 22(5), pp. 728–740, 1977.

[8] L. Huang, J. Song, and C. Zhang, "Observability analysis and filter design for a vision inertial absolute navigation system for uav using landmarks," *Optik*, vol. 149, pp. 455–468, 2017.

[9] G. Panahandeh, S. Hutchinson, P. Handel, and M. Jansson, "Planar-based visual inertial navigation: Observability analysis and motion estimation," *Journal of Intelligent Robotic Systems*, pp. 277–299, 2016.

[10] S. Hong, M. H. Lee, H. H. Chun, S. H. Kwon, and J. L. Speyer, "Observability of error states in gps/ins integration," *IEEE Trans. Veh. Technol*, vol. 54(2), pp. 731–743, 2005.

[11] Y. Tang, Y. Wu, M. Wu, W. Wu, X. Hu, and L. Shen, "Ins/gps integration: Global observability analysis," *IEEE Trans. Veh. Technol*, vol. 58(3), pp. 1129–1142, 2009.

[12] Y. Wu, H. Zhang, M. Wu, X. Hu, and D. Hu, "Observability of strapdown ins alignment: A global perspective," *IEEE Trans. Aerosp. Electron. Syst*, vol. 48(1), pp. 78–102, 2012.

[13] J. Hernandez, K. Tsotos, and S. Soatto, "Observability, identifiability and sensitivity of vision-aided inertial navigation," *IEEE International Conference on Robotics and Automation*, pp. 2319–2325, 2015.

[14] ——, "Observability, identifiability and sensitivity of vision-aided inertial navigation," *25th International Joint Conference Artificial Intelligence*, pp. 4170–4174, 2016.

[15] D. Honegger, L. Meier, P. Tanskanen, and M. Pollefeys, "An open source and open hardware embedded metric optical flow cmos camera for indoor and outdoor applications," *IEEE International Conference on Robotics and Automation*, pp. 1368–1381, 2013.

[16] S. Ibarra, J. Moreno, and G. Espinosa-Perez, "Global observability analysis of sensorless induction motor," *Automatica*, vol. 40(1), pp. 1079–1085, 2004.

[17] P.Batista, C.Silvestre, and P.Oliveira, "On the observability of linear motion quantities in navigation systems," *Systems and Control Letters*, vol. 60, pp. 101–110, 2011.